

METHOD FOR LOCAL MEASUREMENT OF STRESS AND STRAIN IN A FORMED PART UNDER LOAD

M. A. Iadicola¹, T. Foecke¹, and L. Ma¹

¹ NIST Center for Metal Forming
Metallurgy Division, National Institute of Standards and Technology
100 Bureau Drive, Stop 8553, Gaithersburg, MD 20899-855 USA
e-mail: mark.iadicola@nist.gov, Web page: www.nist.gov/msel/metallurgy/materials_performance/

ABSTRACT

The sheet metal forming industry requires prediction of complex deformation processes for various materials and alloys. The use of numerical modeling has been very successful in this regard for well understood and characterized materials being deformed within the characterized envelope. Unfortunately, new materials that require more complex constitutive laws (or are sensitive to particular deformation modes) are not as easily modeled, and in many cases the necessary experimental results do not exist or are quite limited (and do not cover the range of expected deformations, such as high strain under multi-axial loading).

At the National Institute of Standards and Technology (NIST) Center for Metal Forming common test methods (e.g., Marciniak ram test) are being combined with *in situ* X-ray diffraction and full field digital image correlation to determine the local strains and associated stresses during plastic deformations. This new experimental approach can be used to more extensively probe the mechanical response of metal sheets being deformed in multi-axial tension. This paper is intended to introduce the method and present some illustrative examples. Three applications are presented: (1) yield surface determination, (2) benchmark testing, and (3) measurements near a physical feature (in this case asymmetrical expansion of a hole). It is shown that stress-strain behavior can be measured along multi-axial paths, and how local stresses near inhomogeneities can be measured and tracked *in situ* with increasing levels of deformation.

Keywords: Forming; Stress Measurement; Yield Surface; Flow Stress; Multi-axial; X-ray Diffraction; Simulation; Standard Tests.

1. INTRODUCTION

The sheet metal forming industry requires prediction of complex deformation processes for various materials and alloys. For years, experience with familiar materials (e.g., mild steel) permitted empirical correction to predictions to achieve acceptable results, but with the increased rate of alloy development and the decreased time to production (i.e., a year or two of experience rather than decades) more efficient methods are necessary. The use of numerical modeling has been very successful in predicting the behavior for a well understood and characterized material being deformed within the characterized envelope. Unfortunately, new materials that require more complex constitutive laws (or are sensitive to particular deformation modes) are not as easily modeled, and in many cases the necessary experimental results to cover the range of expected deformations (that is high strain under multi-axial loading) are quite limited or do not exist. Various methods of overcoming this problem have been or are being developed (e.g., cruciform testing, benchmark testing, or inverse problem analysis), however these often have to assume a constitutive law and just compare with resulting strains. These methods are further complicated by stress concentrations (e.g., in reentrant corners), friction, and bending, which requires more elaborate modeling and assumptions before the comparison is performed.

At the National Institute of Standards and Technology (NIST) Center for Metal Forming (CMF) common test methods (e.g., Marciniak ram test) are being combined with *in situ* X-ray diffraction (XRD) and full field digital image correlation (DIC) to determine the local strains and associated stresses during plastic deformations. This new, albeit complicated, experimental approach permits determination of multi-axial stress-strain response (to large strains) for various sheet materials without the need for a finite element analysis (FEA) with an assumed constitutive law. The goal is to improve the FEA through better constitutive law selection and calibration.

This paper is intended to introduce the method and present some illustrative examples. After a brief description of the materials to be used for testing, the general experimental procedure associated with Marciniak testing, XRD, and strain measurement is described. Finally, three applications are presented: Example 1 - yield surface determination, Example 2 - benchmark testing, and Example 3 - measurements near a physical feature (in this case asymmetrical expansion of a hole).

2. MATERIALS

In this work, results for aluminum and steel alloys will be discussed, but the methods presented are generally applicable to many common engineering metals. These specific materials are chosen for their interest in the sheet metal forming community. Standard test methods are used to measure the static uniaxial mechanical response of the materials in the typical three directions (rolling direction, RD, transverse to the rolling direction, TD, and on the 45° diagonal to the rolling direction, DD). Different materials are used in each application: AA5754-O for Example 1; AA6022, AKDQ, HSLA50, and DP600 for Example 2; and a different HSLA50 for Example 3. Table 1 lists the basic material properties including: 0.2 % offset yield stress (YS), ultimate tensile strength (UTS), uniform elongation (UE), thinning ratio (r), and the parameters (n and K) for a simple power-law hardening model ($\sigma = K\varepsilon^n$) relating strain (ε) to stress (σ). Note that AA5754-O exhibits the Portevin-Le Chatelier (PLC) effect, and both HSLA materials exhibit yield point behavior. Uniform elongation for both of these alloys has been redefined (to ignore the continuous localization of the PLC effect and the initial localization of the HSLA) to

be at the overall maximum of the smoothed engineering stress-strain curve during the later stages of hardening (see [1-2] for further details).

Table 1. Material properties for all materials discussed in Section 4. Data (and available uncertainties, shown in brackets) are taken from [1-3] for all but 1.00 mm thick HSLA50.

Material (thickness)	Direction	YS (MPa)	UTS (MPa)	UE (%)	r	K (MPa)	n
AA5754-O (1.00 mm)	RD	94.1 [3.3]	226 [3]	18.9 [0.9]	0.69 [0.02]	474 [9]	0.317 [0.010]
	TD	92.1 [0.7]	218 [1]	21.5 [0.5]	0.87 [0.02]	458 [6]	0.326 [0.006]
	DD	90.9 [0.6]	216 [3]	22.4 [0.9]	0.73 [0.03]	447 [3]	0.323 [0.004]
AA6022 (1.00 mm)	RD	136.0	256.9	22.2	1.029	479.9	0.258
	TD	127.6	238.3	24.0	0.728	442.5	0.258
	DD	131.2	247.6	24.8	0.532	455.0	0.254
AKDQ (1.00 mm)	RD	158.3	315.0	26.4	1.546	579.9	0.256
	TD	166.0	312.0	24.6	1.942	569.0	0.250
	DD	164.7	317.0	25.1	1.508	579.7	0.252
HSLA50 (0.79 mm)	RD	394.3	463.7	16.4	0.581	770.0	0.187
	TD	427.7	466.0	17.5	1.013	758.7	0.176
	DD	395.3	447.0	17.0	1.166	733.0	0.182
DP600 (0.98 mm)	RD	420.0	688.7	14.0	0.821	1080.7	0.152
	TD	425.7	697.0	13.5	0.969	1090.3	0.151
	DD	427.7	690.7	12.8	0.915	1078.2	0.150
HSLA50 (1.00 mm)	RD	364 [5]	427 [5]	19.1 [0.5]	1.03 [0.05]	597 [18]	0.105 [0.010]
	TD	392 [5]	435 [5]	17.5 [0.5]	1.36 [0.10]	594 [14]	0.093 [0.010]
	DD	376 [7]	428 [5]	18.2 [0.5]	1.33 [0.12]	568 [19]	0.081 [0.010]

3. EXPERIMENTAL PROCEDURE

3.1 Marciniak testing

In addition to the standard uniaxial deformation used in the previous section, this work uses an augmentation of the Marciniak flat ram test [4] to deform the specimen in multi-axial tension. The method uses as-received sheet metal samples that are trimmed down to specific widths to impose specific nearly linear strain ratios [5]. Figure 1 is a top view and through-section of the axisymmetric die, binder, and ram (with a center recess). Square samples of approximately 305 mm on each side result in equi-biaxial (EB) deformation, and very thin strips deform uniaxially. Strain ratios between these two extremes (e.g., plane-strain, PS) are achieved by reducing the widths from the square sample to the thin strip, resulting in reduced straining in the reduced width direction. A reinforcement washer (typically made of a mild steel sheet with a centered 32 mm hole) is used to reinforce the sheet along the bend of the ram and die radii, thus forcing deformation in the center of the sample above the center of the ram. Vegetable based oil lubricant is applied to the top surface of the sample where it contacts the die and the bottom surface of the washer where it contacts the ram bead. Columns and additional rings, not shown in

Figure 1, reinforce the die ring. This leaves the top of the specimen (above the center of the ram) accessible for the metrology that will be described in the following sections. A lock-bead (see Figure 1) is used in all of the testing presented here. Procedurally, after specimen and washer insertion between the die and binder (Figure 1, through-section), the die is lowered into place and the binder is clamped to a selected force (setting the lock-bead, before the ram is positioned to lightly touch the sample). Ram displacement is controlled throughout the test, where the ram may be displaced continuously or to selected levels (interrupted testing) and held there for hours. Ram and clamp loads and positions are continuously monitored during the tests.

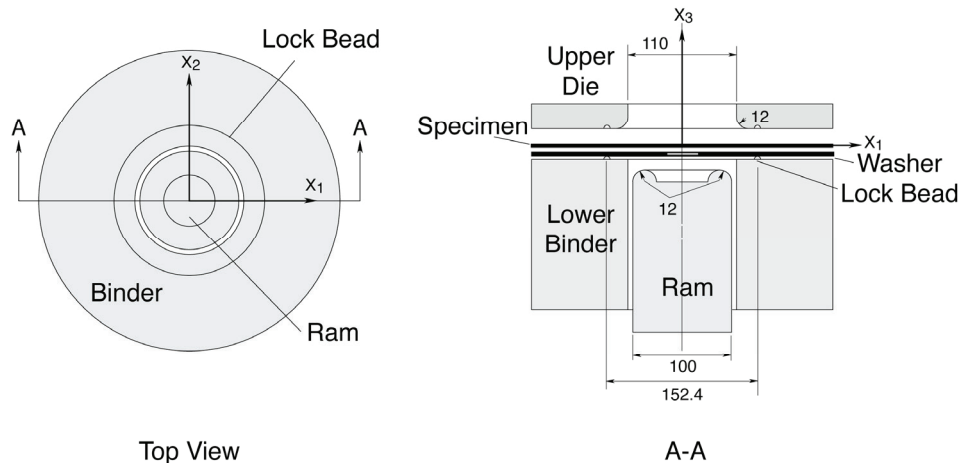


Figure 1. Top view and through-section (with specimen and washer inserted) of axisymmetric ram, binder, and die (dimensions shown in mm).

3.2 Strain measurement

Two methods of strain measurement are employed in the examples that follow: mechanical extensometry and DIC. Early work (Example 1) used a specially made miniature biaxial mechanical extensometer (with a 12 mm by 12 mm footprint on the top face of the sample). This device is designed to travel with the top surface of the sample (attached by elastic bands) and permits continuous strain measurement (at Class C or better accuracy, ASTM E83-92, throughout the 40 % strain range) in two orthogonal directions averaged over the gage length between the extensometer knife-edges. Layout lines drawn on the surface of the sample permit alignment of the axes of the extensometer to the RD and TD of the sample. Unfortunately, the device can be easily bumped during other surface measurements being made during a test, therefore in Examples 2 and 3 the extensometer is replaced by a non-contacting commercial 3-D DIC system.

The 3-D DIC system uses two cameras to acquire stereo-images of the top surface of the sample. Through 3-D photogrammetry, the displacements of a random surface pattern (painted black dots on a white base coat) are tracked from the reference image pair to the current image pair in all three dimensions. These displacements are then used to calculate full-field surface strains. Strains at specific spots of interest on the surface are then interpolated from these data. To synchronize the measured strains to the test, the DIC system incorporates an analog to digital data acquisition system that acquires the control signals of the machine at the time of image acquisition. Calibration of the system is checked frequently using a series of images taken of a reference target in various positions. Precision is dependent on multiple image processing

parameters, but in general the strain resolution in the examples shown here is on the order of 200 micro-strain to 400 micro-strain. In Examples 2 and 3, small areas on the surface of the sample do not have a painted pattern. These exposed areas are required for the XRD measurements (to be described next). The smoothness of the strain fields is verified with other fully painted samples, and permits confident approximation of the strains at the masked points by interpolating from the neighboring areas where data is available.

3.3 X-ray diffraction measurements

XRD is performed on a small spot on the surface of the sample during testing to measure the interatomic lattice spacing, and through calibrated X-ray elastic constants (XECs), determine the macroscopic stress in the sample. This method assumes that the material has been sufficiently plastically deformed to remove any residual stress from earlier processing (e.g., skin pass through thickness residual stress). The measurement technique is based on methods developed to measure residual stresses [6], and is reviewed briefly here. Bragg's law relates the lattice spacing (d) of a crystalline material to the wavelength (λ) of the source X-rays and the reflected angle (2θ), therefore a change in lattice spacing will result in a change in the angle of reflection (for all other parameters held fixed). With multiple crystallites in the reflecting volume of material, multiple d -spacings are measured simultaneously over a range of reflection angles. These measurements form a distribution of intensity for changes in the reflection angle. This distribution is commonly referred to as a diffraction peak, and the top portion of this peak is fit to an appropriate function. By measuring the change in the diffraction peak position for a specific family of lattice planes of interest ($\{hkl\}$) the change in lattice plane spacing can be monitored. If the reference stress-free lattice spacing (d_o) is known (usually measured on a fine powder of the same material), then a lattice strain can be calculated which relates to the stress in the crystal through XECs. A key point to understand is that the crystal lattice experiences elastic strains only. Plastic strain will cause increased dislocation density and dislocation motion, which can broaden the peak, but will not change the peak position.

Figure 2a defines the axes for the specimen surface system (X_i) and the X-ray beam and detector system (\hat{X}_i) where \hat{X}_3 is the bisector of the incident and reflected beams (Figure 2b). The rotation angles between the systems are ϕ (in-plane rotation angle) and ψ (tilt from the surface normal, X_3 , about the \hat{X}_2 axis). The standard definition of the average lattice strain in the \hat{X}_3 direction is

$$e'_{33} = \frac{d_{\phi\psi} - d_o}{d_o}, \quad (1)$$

where $d_{\phi\psi}$ is the lattice spacing at a specific pair of rotation angles. After rotation of the lattice strain to the surface system Equation 1 in terms of surface strain would be

$$\begin{aligned} \frac{d_{\phi\psi} - d_o}{d_o} = & \varepsilon_{11} \cos^2 \phi \sin^2 \psi + \varepsilon_{12} \sin(2\phi) \sin^2 \psi + \varepsilon_{22} \sin^2 \phi \sin^2 \psi \\ & + \varepsilon_{33} \cos^2 \psi + \varepsilon_{13} \cos \phi \sin(2\psi) + \varepsilon_{23} \sin \phi \sin(2\psi) \end{aligned} \quad (2)$$

If an isotropic constitutive relationship is assumed for the lattice (as is typical in this type of analysis) the surface strain components can be replaced by stresses with the introduction of two XECs S_1 and S_2

$$\begin{aligned} \frac{d_{\phi\psi} - d_o}{d_o} = & \frac{1}{2} S_2 \{ \sigma_{11} \cos^2 \phi + \sigma_{12} \sin(2\phi) + \sigma_{22} \sin^2 \phi - \sigma_{33} \} \sin^2 \psi \\ & + \frac{1}{2} S_2 \{ \sigma_{13} \cos \phi + \sigma_{23} \sin \phi \} \sin(2\psi) + \frac{1}{2} S_2 \sigma_{33} + S_1 \{ \sigma_{11} + \sigma_{22} + \sigma_{33} \} \end{aligned} \quad (3)$$

The constants S_1 and S_2 are dependent on material composition, lattice direction (hkl), and other microscopic effects, and can be calibrated experimental or occasionally found in the literature [6]. The XECs used in the examples to follow are calibrated experimentally from material in the same batch, and will be referred to as effective X-ray elastic constants (EXEC) for clarity.

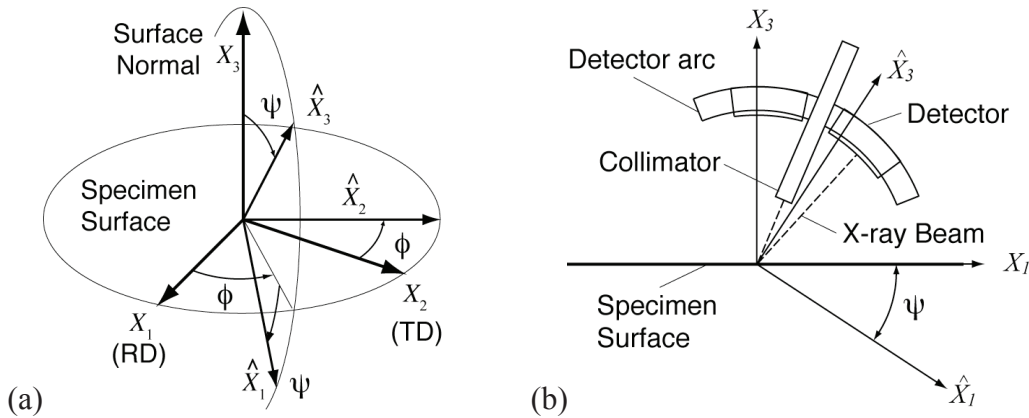


Figure 2. XRD axis definition: (a) for surface, X_i , and detector, \hat{X}_i , systems; and (b) simplified case for $\phi = 0$ showing \hat{X}_3 as bisector of reflected beam angle for right-side detector.

In addition to the EXEC and d_o , the XRD measurement of stress at any given stress state requires measurement at a proper variety of angle pairs to solve for the six unknown stresses. Over-sampling is preferred to permit an analysis of uncertainty. Certain assumptions can quickly reduce the number of unknowns, and thus reduce the required number of sampled angle pairs. Here are two cases using some common assumptions. For Case 1, if we assume that $\sigma_{33} = 0$ for a thin sheet being deformed by in-plane tension, then the stress-free lattice spacing (d_o) can be calculated from the measured data (reducing Equation 3 by one unknown). Additionally, for Case 2, if we assume that the principal stresses align with the principal strain axes for rolled material loaded in the RD or TD, then only measurements at $\phi = 0^\circ$ and $\phi = 90^\circ$ are needed to determine the in-plane stresses. Case 1 is assumed for Examples 2 and 3, below, where a range of ϕ -angles and ψ -angles are sampled to solve for the remaining five components of stress. Case 2 is used for Example 1, below, where $\phi = 0^\circ$ or $\phi = 90^\circ$ and a range of ψ -angles are scanned to measure σ_{11} and σ_{22} only.

For the aluminum samples, a Co X-ray source is used on the as-received sample surface. For all of the steels tested, a Cr X-ray source is used, and the surface has the zinc coating removed. The paint used for DIC can degrade the X-ray signal and affect the focus distance, therefore the

area for XRD was masked from painting and results in a small gap in the strain field data. As mentioned in the Section 3.2 the smooth strain fields allow interpolation through these areas. The size of the XRD measurement area on the surface is set by selection of an appropriate aperture for the end of the beam collimator (for Example 1: 5 mm by 1.5 mm, for Example 2: 2 mm diameter and for Example 3: 1 mm diameter).

4. RESULTS AND DISCUSSION

In this section, three examples using the unique measurement methods described above are presented. In each case a brief background and description of the experiment involved is given, followed by a description of some of the particulars of the procedure, and culminate with highlights from the results.

4.1 Example 1: Yield surface determination

Traditional methods of multi-axial sheet metal testing (namely cruciform or uniaxial wide-sheet testing) require FEA to determine the stress, based on the measured load and a correction factor. The method described here (and in greater detail in [1]) is intended to determine these data less ambiguously by not requiring the assumption of a plastic constitutive law *a priori*. The use of the Marciniak testing can achieve large multi-axial strains (EB to above 20 % and PS to almost 15 %) well above that of the other methods (e.g., < 5 % for cruciform).

The procedure follows that described in Section 3.1, with interrupted straining by stepping the ram at quasi-static rates (0.1 mm/s) followed by a hold under load during XRD focusing and scanning (taking about 8 minutes total time for each step in the ram). XRD scanning includes 26 ψ -angles between -37.4° and $+37.4^\circ$ in one ϕ -angle direction (either RD or TD). This method of testing requires two tests for each strain path (i.e., EB, PS, etc.), one in RD and one in TD. In addition, each individual test was repeated (by different system operators, about one month apart) to verify the repeatability of the measurements. By tilting in only one direction during each test, the mechanical extensometer could be attached near the XRD head parallel to the tilt direction, but just beyond the diffraction spot. The strain measured by the extensometer is averaged during each position hold, and is seen to vary by <0.005 % strain during the XRD scan. EXEC are determined from uniaxial testing with a series of unloads [7]. Results of uniaxial XRD measurements are compared to the results from continuous uniaxial testing in Figure 3a for the RD. The agreement is seen to be excellent.

Figure 3b plots the true stress vs. true strain results for EB, PS, and uniaxial testing using the XRD system for the RD direction. The measured uncertainties (approximately the size of the data symbols in Figure 3b) are based the quality of the linear fit of the $\sin^2 \psi$ term in Equation 3, and are about the same amplitude as the variation of the stress due to the PLC effect as seen in the hardening curve of Figure 3a. From these data (and similar for tests performed in the TD direction), the stress values at equal plastic work levels (equivalent to the work at 1 %, 5 %, 10 % and 15 % uniaxial RD strain levels) are calculated for all three strain paths in RD and TD. These results are plotted in Figure 3c along with two fits to an eight-parameter model (Yld2000-2d, [9]) based on (1) the measured strain ratio r -values or (2) using optimized r -values based on the 15 % data points. Even using this rather advanced model the fit to the data does not capture the PS behavior without using optimized (artificially high) r -values. Additionally, the fits do not capture the changing EB behavior between the 1 % and 15 % levels. These seemingly peculiar large EB stress values, with stress ratios not equal to 1, are in a range of strain rarely achieved by

other test methods (except pressurized tube tests). One such tube test method [9] shows similar behavior, also with a stress ratio >1 .

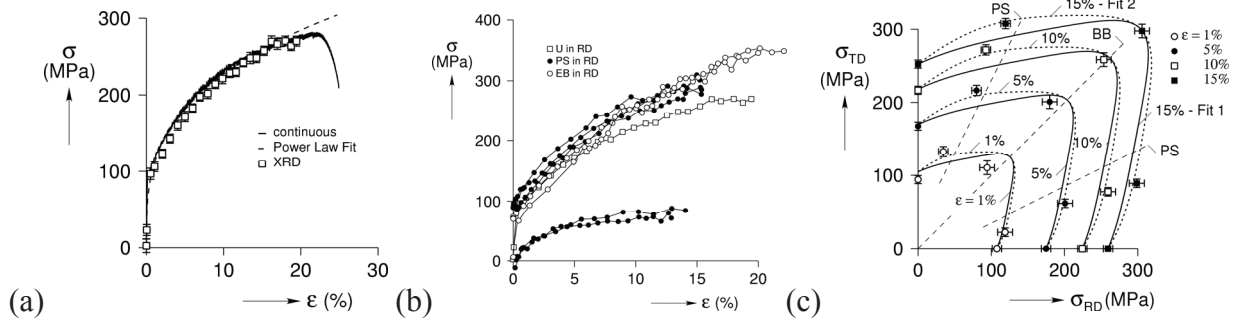


Figure 3. Example 1 results (from [1]) (a) comparison of continuous uniaxial test with XRD data, (b) multi-axial true stress-true strain data for RD, and (c) equal work data with Yld2000-2D yield curves based on measured r -values (Fit 1) and optimized r -values (Fit 2).

4.2 Example 2: Benchmark testing

The third benchmark of Numisheet 2005 conference “Channel Draw/Cylindrical Cup Benchmark” [10] includes a two stage forming process and uniquely requires the measurement and prediction of *in situ* stress, in addition to surface strains. Stage 1 is a channel draw process with variable draw bead depth, resulting in a cyclic bend/unbend deformation followed by plane straining in the sheet TD. This results in a sizable springback in the side-walls. Stage 2 (which will be discussed in this section) cuts curved samples out of these side-walls and subjects them to plane strain by the method described in Section 3.1 to specified ram heights, at which point the position is held and sample stress is measured above the center of the ram by XRD. Another interesting aspect of the benchmark is that the Stage 2 samples are oriented in two directions: Shape A approximates PS at a right angle to the plane straining of Stage 1, and Shape B continues the PS deformation in same direction as Stage 1. The original 2005 benchmark required results [11-12] and predictions for one bead depth for four materials (the AA6022, AKDQ, HSLA50, and DP600 in Table 1). The extended benchmark (completed recently) required these same measurements for four bead depths and as-received samples for all four materials [13-14]. Unfortunately, the AA6022 had aged too long and its results are no longer considered true to the original benchmark design. The details of the testing are beyond the scope of this work (and may be found in [14]), but some of the more interesting results are described here. The benchmark testing requires that a minimum of three tests be performed for each condition to check variability of the results. Therefore, in excess of 100 tests were performed, with only a very small subset described here.

Nominally 254 mm by 135 mm samples are cut from the curved side-walls of the Stage 1 channel draw samples after springback. Shape A samples are cut perpendicular to the curvature of the sheet, and Shape B samples are cut parallel to the curvature of the sheet [12]. Flattening of these samples is part of the benchmark process, and is accomplished by closing of the die (Figure 1) on the sample prior to clamping (to set the lock bead). After clamping, the ram is lightly preloaded (0.2 kN) and then raised (at 1 mm/s) to a benchmark specified level slightly below failure [12] and held at that position. The XRD head is focused and a series of 14 ψ -angles at 4 ϕ -angles are scanned, in less than 15 minutes. These data are used as described in Section 3.3 to determine d_0 and the five stress components of interest. EXEC are determined for

each material by performing elastic 4-point bend tests on a 135 mm by 20 mm sample that is instrumented with a calibrated foil strain gage. A minimum of five loading and unloading points are used for each calibration curve.

The results of the testing showed higher than normal variability in strain and stress between samples for certain test conditions and certain alloys. For instance, the strain results for three repeated Shape A AKDQ samples for each of the three highest draw-bead depths show much higher variability (averaging $> 2.5\%$ strain) than the other AKDQ samples (averaging $< 1\%$ strain) and other steels (typically $< 1\%$ strain). Similarly large variations are seen in the measured stress results. Recall that, in this case, the strain history of the samples has a perpendicular path change from Stage 1 to 2 testing. The result is a localization of the deformation, which can have a large effect on the measured stresses and strains. Figure 4 shows the first principal true strain map for three AKDQ samples (Shape A as-received, Shape A Stage 1 bead depth penetration of 75 %, and Shape B also at Stage 1 bead depth of 75 %). The localization (neck) is clearly visible in Figure 4b (and when the sample is visually inspected after testing). Not surprisingly, stress measurements are location sensitive near a feature that results in a large gradient in stress. Another interesting case is the large variability in the stress results for HSLA samples for Shape A, which on average are twice that of the HSLA Shape B samples (for all the Stage 1 conditions). Figure 5a and 5b are perspective plots of two HSLA samples both from the same Stage 1 draw bead penetration depth, but cut down to Shape A and B, respectively. A periodic roughening is clearly visible, and can be felt on the part after testing. Stress measurement in this oscillating strain field will be quite position sensitive.

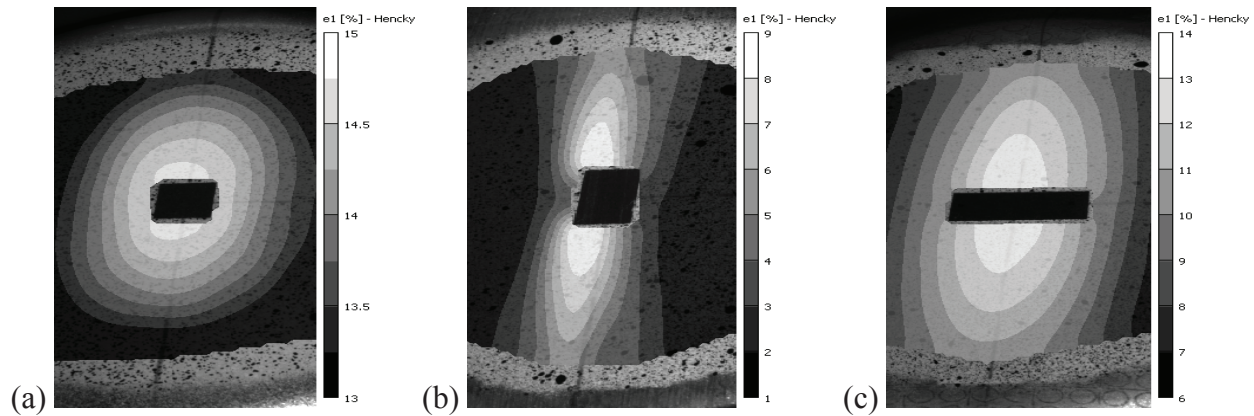


Figure 4. First principal true strain fields for AKDQ samples (a) Shape A as-received (b) Shape A 75 % bead depth and (c) Shape B 75 % bead depth.

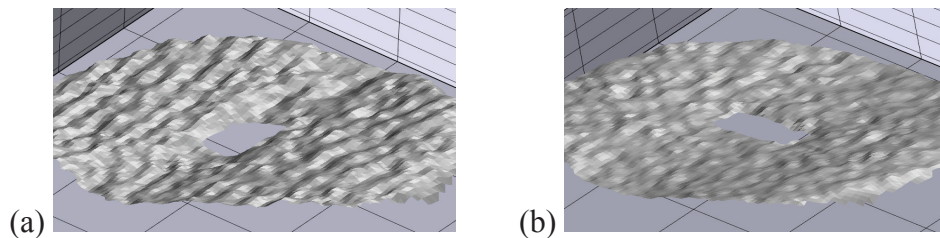


Figure 5. Perspective plot of DIC measured surface heights for HSLA 50 samples for 50 % Stage 1 bead depth: (a) Shape A and (b) Shape B.

The testing method's sensitivity to these features is seen as a testimony to its overall sensitivity and applicability. To show this point more clearly, a test with a specific physical feature with a known location is of interest. This idea leads into the next example.

4.3 Example 3: Asymmetric hole expansion

Our final example is a preliminary look at a more complex test. A physical feature is considered that will simultaneously produce a variety of strain paths and a stress field with measurable variation. The same Marciniak method as described in Section 3.1 is used here except a small (6.35 mm diameter) hole is drilled 12 mm off the center of the 305 mm x 305 mm HSLA sheet sample in the RD (see Figure 6a). The hole edge is deburred and sanded smooth after machining (similar to the washer hole, dashed line in the figure). In Figure 6a, the points (A, B, and C) located at the origin and at 5 mm offsets along the RD are the locations used for stress measurement. Similar to Example 2, the spots used for XRD have the zinc coating removed and are masked from the DIC paint pattern leaving small (2.5 mm diameter) areas lacking strain measurement (Figure 6b). After a preliminary test to failure, five ram heights are selected for position holds and XRD measurements. A similar procedure to the earlier examples is followed with an added step of repositioning and refocusing to each of the three measurement points (A, B, and C). Figure 6b is the strain field plot measured during the third position hold. A comparison of the strain fields between the XRD test (with holds) and the preliminary (continuous rate) test, shows the field measured with the missing data (at A, B, and C) is consistent with the field measured for the preliminary test.

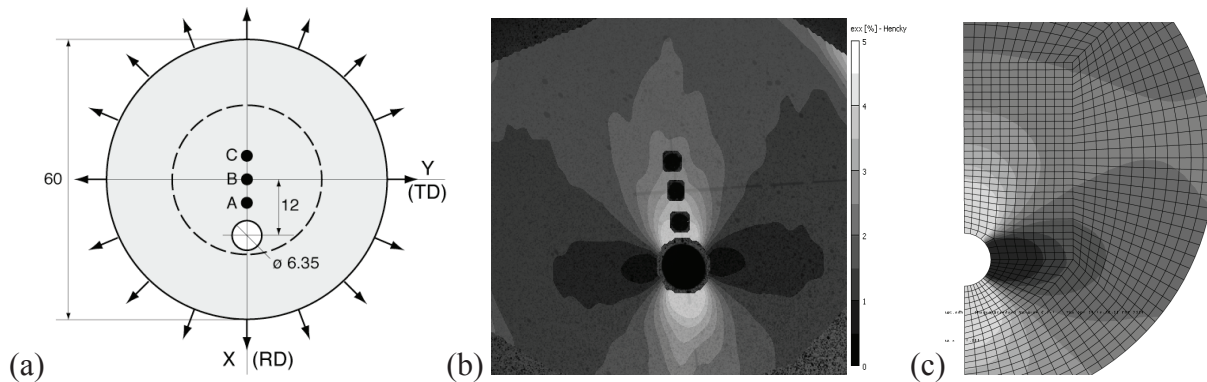


Figure 6. Example 3: (a) drawing of the geometry (dimensions in mm), (b) measured ε_y strain map for hold position 3, and (c) FEA calculated strain map at a similar strain level (plotted in same gray scale).

An ABAQUS/Standard FEA of the test is performed using the dimensions shown in Figure 6a. Only half of the part (TD positive) is modeled with symmetry conditions along the RD axis. Four node plane-stress elements (1105 elements with 1173 nodes) with bilinear interpolation are used. The material is modeled with a combined elasto-plastic formulation. The elastic behavior is treated as isotropic with a 209 GPa elastic modulus and 0.28 Poisson's ratio. The plastic hardening curve is taken directly from the uniaxial RD data with minor adjustment to the data at the yield point and subsequent plateau (this region is made positive definite, with a slope of 507 MPa, to prevent numerical complications). The plastic anisotropy is modeled using the Hill'48 formulation (based on the r -values given in Table 1). The loading is applied as a uniform radial displacement, as shown in Figure 6a, in steps chosen to approximate the experimental results for ε_y along the X -axis near A, B, and C.

Figure 6c shows the FEA predicted strain field for a displacement level similar to the test point shown in Figure 6b. Qualitatively, the results are consistent, and the location of the initial plastic behavior around the hole is consistent between the model and test. Unfortunately, the model prediction for step 5 shows localization of strain near the hole that is not present in the measurements, but the location along the hole is consistent with the area of eventual failure seen in the experiment. Therefore, the model can capture much of the test results, however a quantitative comparison of the FEA and measured results is not as favorable. Figure 7a and 7b are plots of the true strain (ε_Y and ε_X , respectively) variation along the X -axis (Figure 6a) for steps 1 through 4. Uncertainties of the DIC data are smaller than the symbols used. The three gaps (outside of the hole region) in the measured strain data are at the points A, B, and C. The FEA and experimental results match well in the region of points A, B, and C (Figure 7a) since this is the data used to define the FEA steps, but the far field strains do not necessarily match (particularly $X < -10$ mm). The ε_X data along this same axis (Figure 7b) also captures the correct trends, but the values of true strain differ from the FEA and experiment (again greatest in the far field). Although a comparison of the stresses show they are off by an even greater amount, the FEA and measured stress values are all tensile and properly capture the spatial trends between points A, B and C. This quantitative disparity in stress might partially be the result of a recent experimental issue with the testing machine, which shows a loss of pressure at the hold points (unloading the sample by 3 %). These technical issues are currently being addressed, but assuming the small unloading results in a small (uniform) elastic unloading, the measured stress ratio may still be useful. A comparison of the measured (points) and FEA predicted (lines) stress ratio (σ_Y/σ_X) is shown in Figure 7c. Although the general decrease of the stress ratio away from the hole is captured, the expected step-to-step variation is not correct. Steps 1 and 2 in the range of yield point behavior seem to follow a single trend with measured stress ratios generally greater than the FEA calculated ratios, and steps 3 and 4 follow the reverse trend with measured ratios generally below the FEA calculated values. The results at point A do not necessarily follow these trends, but also have the largest associated uncertainties, being in a region of severe stress gradients. Not surprisingly, application of the method in regions with high gradients might require some additional analysis. If the measured stresses are low due to the unload, increasing both stress values will bring the ratios closer to unity and closer to the FEA results for steps 1 and 2, but further from the FEA results for steps 3 and 4. Therefore more investigation after correction of the technical issues is required to determine if there is a disproportionate unloading occurring in the test results presented here, or if there is an error in the FEA predicted stresses (and thus a problem with the assumed material model).

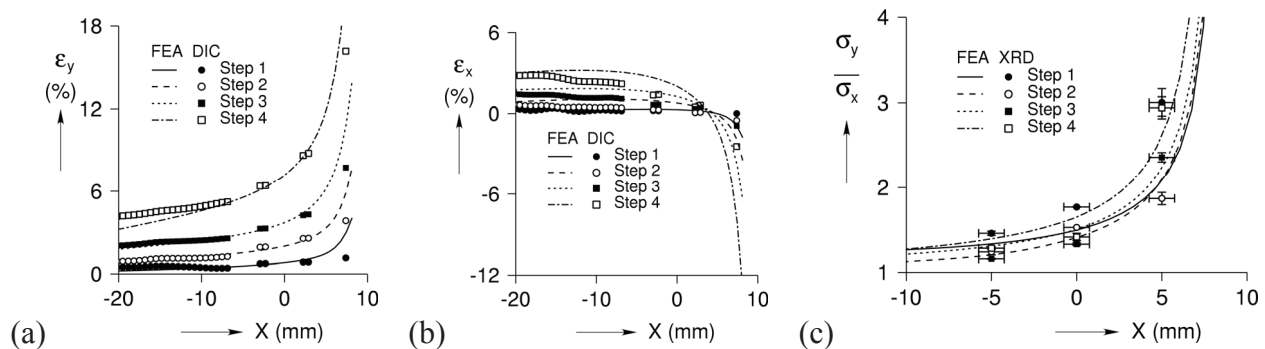


Figure 7. Stress and strain variation along the X -axis for Example 3: (a) ε_Y , (b) ε_X , and (c) stress ratio σ_Y/σ_X . FEA results are shown as lines and measured data as points.

5. CONCLUSIONS

In this paper we have detailed newly developed experimental capabilities that can be used to more extensively probe the mechanical response of metal sheets being deformed in multi-axial tension. Not only can stress-strain behavior be measured along multi-axial paths, but also local stresses near inhomogeneities can be measured and tracked *in situ* with increasing levels of deformation. It is believed that further development of these techniques will lead to both new standard tests for sheet behavior and a better fundamental understanding of multi-axial forming behavior.

6. REFERENCES

1. M.A. Iadicola, T. Foecke, and S.W. Banovic: “Experimental observations of evolving yield loci in biaxially strained AA5754-O”, *International Journal of Plasticity* 24 (2008) 2084-2101.
2. M.F. Shi and M. Huang: “Specification for benchmark materials”, *Numisheet 2005 Part B* (2005) 1173-1178.
3. J.C. Brem, F. Barlat, R.E. Dick, and J.-W. Yoon: “Characterization of aluminum alloy sheet materials Numisheet 2005”, *Numisheet 2005 Part B* (2005) 1179-1190.
4. Z. Marciniak and K. Kuczynski: “Limit strains in the processes of stretch-forming sheet metal”, *International Journal of Mechanical Science* 9 (1967) 609-620.
5. K.S. Raghavan: “A simple technique to generate in-plane forming limit curves and selected applications”, *Metallurgical and Materials Transactions A* 26A (1995) 2075-2084.
6. I.C. Noyan and J.B. Cohen: *Residual Stress: Measurement by Diffraction and Interpretation*. Springer-Verlag (1987)
7. M.A. Iadicola and T.H. Gnaeupel-Herold: “In situ stress measurement of biaxially strained AA5754-O”, *Advances in X-ray Analysis* 51 (2008) 131-137.
8. F. Barlat, J.C. Brem, J.W. Yoon, K. Chung, R.E. Dick, D.J. Lege, F. Pourgoghrat, S.H. Choi, E. Chu: “Plane stress yield function for aluminum alloy sheets – Part 1: theory”, *International Journal of Plasticity* 19 (2003) 1297-1319.
9. T. Kuwabara, K. Yoshida, K. Narihara, and S. Takahashi: “Anisotropic plastic deformation of extruded aluminum alloy tube under axial forces and internal pressure”, *International Journal of Plasticity* 21 (2005) 101-117.
10. T.B. Stoughton, D. Green, and M. Iadicola: “Specification for BM3: two-stage channel/cup draw”, *Numisheet 2005 Part B* (2005) 1157-1172.
11. D.E. Green: “Description of numisheet 2005 benchmark #3 stage-1: channel draw with 75 % drawbead penetration”, *Numisheet 2005 Part B* (2005) 894-904.
12. M.A. Iadicola, T. Foecke, and T.B. Stoughton: “Experimental procedures and results for benchmark 3: stage 2 forming process”, *Numisheet 2005 Part B* (2005) 905-915.
13. D.E. Green, T.B. Stoughton, T. Gnaeupel-Herold, M.A. Iadicola, and T. Foecke: “Influence of drawbeads in deep drawing plane-strain channel sections” *Proceedings of IDDRG 2006 Porto Portugal* (2006) 559-566.
14. M.A. Iadicola and T. Foecke: “Extended results for Numisheet 2005 channel draw/cylindrical cup benchmark”, (to be submitted for NIST report)